Front. Earth Sci. 2016, 10(1): 38–48
DOI 10.1007/s11707-015-0510-y

RESEARCH ARTICLE

Air temperature field distribution estimations over a Chinese mega-city using MODIS land surface temperature data: the case of Shanghai

Weichun MA, Liguo ZHOU, Hao ZHANG, Yan ZHANG, Xiaoyan DAI (✉)

Department of Environmental Science and Engineering, Fudan University, Shanghai 200433, China

Abstract The capability of obtaining spatially distributed air temperature data from remote sensing measurements is an improvement for many environmental applications focused on urban heat island, carbon emissions, climate change, etc. This paper is based on the MODIS/Terra and Aqua data utilized to study the effect of the urban atmospheric heat island in Shanghai, China. The correlation between retrieved MODIS land surface temperature (LST) and air temperature measured at local weather stations was initially studied at different temporal and spatial scales. Secondly, the air temperature data with spatial resolutions of 250 m and 1 km were estimated from MODIS LST data and in-situ measured air temperature. The results showed that there is a slightly higher correlation between air temperature and MODIS LST at a 250 m resolution in spring and autumn on an annual scale than observed at a 1 km resolution. Although the distribution pattern of the air temperature thermal field varies in different seasons, the urban heat island (UHI) in Shanghai is characterized by a distribution pattern of multiple centers, with the central urban area as the primary center and the built-up regions in each district as the sub-centers. This study demonstrates the potential not only for estimating the distribution of the air temperature thermal field from MODIS LST with 250 m resolution in spring and autumn in Shanghai, but also for providing scientific and effective methods for monitoring and studying UHI effect in a Chinese mega-city such as Shanghai.

Keywords air temperature, land surface temperature, urban heat island, MODIS, Shanghai

1 Introduction

There is growing concern for various adverse environmental effects caused by rapid urbanization, not the least of which is the formation and evolution of the urban heat island (UHI). The UHI effect correlates closely to urban land cover change and human socio-economic activities, which may be reflected as a change in urban ecological and environmental conditions. During the past 20 years, UHI effect has been recognized as a major public hazard, detrimental to social and economic development and public health in cities. The UHI effect could possibly lead to more frequent heat strokes, an increase in energy consumption, and may induce photochemical smog pollution and a turbidity island effect. As a result, the UHI effect has been the source for major concerns across both academic and governmental institutions, as well as to the public as a whole in recent decades.

With the advancement of sensor technology, land surface temperature (LST) retrieval from thermal infrared band data of remote sensors has become one of the major approaches for studying the UHI effect (Owen et al., 1998; Weng, 2009). Use of remotely sensed data gives the advantages of wide scope, periodical overpass at a comparatively low-cost, and can provide the information needed on spatio-temporal distribution of UHI for a city, covering the entire urban area at the same time (Sobrino et al., 2012).

To date, most research conducted on the UHI has been based on the LST retrieved from remotely sensed thermal infrared (TIR) data, which provide a unique source of information to assess the surface heat island effect (Weng, 2009). However, near surface air temperature is also a key environmental variable in a wide range of applications within ecology, hydrology, as well as climate and atmospheric sciences. Air temperature is measured from weather stations with high accuracy and high temporal

Received September 18, 2014; accepted December 1, 2014

E-mail: xiaoyandai@fudan.edu.cn

resolution; however, the availability of spatial information on air temperature is often limited. The capability for obtaining truly distributed air temperature data from remote sensing measurements has greatly improved for many environmental applications, such as ecological modeling, etc. (Stisen et al., 2007). More and more researchers try to utilize remotely sensed TIR data with higher temporal and spatial resolution to study the urban atmospheric heat island effect. There are currently three approaches that can be used to estimate air temperature from remotely sensed data: 1) Temperature Vegetation Index (TVX) method (Qi et al., 2005; Stisen et al., 2007), 2) neural network technique (Jang et al., 2004; Mao et al., 2008), and 3) empirical statistical methods. According to the strong correlation between LST and air temperature, empirical statistical methods generally build the empirical equations between air temperature from meteorological station observations and LST or brightness temperature of the corresponding pixel using statistical methods, such as linear regression analysis. The regression equations are then applied to derive the air temperature for the entire study area. Zhou et al. (2001) set up the empirical relations between air temperature and brightness temperature for urban built-up area, industrial zones, suburban area, and agricultural zones in rural area, with correlation coefficients between 0.87 and 0.99. Jones et al. (2004) estimated minimum air temperature from Moderate Resolution Imaging Spectroradiometer (MODIS) Aqua LST by establishing the linear regression equations between nighttime LST and minimum air temperature for different terrain types. The resultant root mean square error (RMSE) ranged from 0.15°C to 0.74°C, and the estimated air temperature had an overall average correlation (COR) of 0.71, indicating that the spatial variation in estimated temperature agreed well with the spatial variation in observed minimum temperature. Colombi et al. (2007) developed the linear regression equations between MODIS LST and air temperature to derive daytime and nighttime air temperature in the Alpine area, with resultant RMSEs of 2.47°C, 3.36°C, and 1.89°C for daytime, nighttime and daily mean temperatures, respectively.

Research studies have also indicated that the effectiveness of estimation using statistical methods is not the same for all seasons. Liu et al. (2010) analyzed the correlation between air temperature recorded at weather stations from 2004 to 2006 and MODIS brightness temperature in Sichuan province with multiple time scales. The results indicated that there was a higher correlation between average monthly brightness temperature and average monthly air temperature, but a lower correlation between average daily brightness temperature and average daily air temperature. Fu et al. (2011) estimated the air temperature of an alpine meadow on Northern Tibetan Plateau at heights of 1.5−2.1 m using MODIS LST data. The results showed inaccurate linear estimations of daily maximum and daytime mean air temperatures from MODIS LST data during the growing season (from May to mid-October); however, the linear relationships between daily maximum and daytime mean air temperatures and MODIS LST during the non-growing season (from mid-October to April) were both significant. Zakšek and Schroedter-Homscheidt (2009) developed a parameterization that derived air temperature with high spatial (1 km) and temporal resolution (30 min) from SEVIRI and MODIS data. A downscaling procedure from the SEVIRI pixel resolution of several kilometers to a 1km spatial resolution was performed using a regression analysis between LST and NDVI acquired by the MODIS instrument, and the lapse rate between the LST and air temperature was removed using a parameterization that required albedo, down-welling surface short-wave flux, relief characteristics, and NDVI data. The results indicated that the parameterization was valid for Central Europe; however, the resultant root mean square deviation fluctuated month to month.

Shanghai, an international metropolis and the flagship of China's economy, has experienced rapid urbanization since the 1990s. With rapid urban expansion and robust socio-economic development in Shanghai, the change of thermal environment, represented by UHI effect, is directly affected by intensifying human activities, increasing built-up areas, and regulation of industrial distribution (Qi, 2004; Shi et al., 2009; Dai et al., 2010). To explore the spatial distribution characteristics of urban atmospheric thermal environment in Shanghai for this paper, air temperature data with spatial resolutions of 250 m and 1 km were estimated from MODIS LST data and air temperature measured from weather stations. To discuss the effectiveness of estimation, the correlation between retrieved LST and measured air temperature was studied for different seasons. Based on these results, a comparison of the spatial pattern of air temperature thermal field and LST thermal field in Shanghai was discussed to provide scientific and effective methods for monitoring and studying urban heat island in the mega-city of Shanghai, China.

2 Study area and data sources

2.1 Study area

Shanghai lies between 30°23′−31°37′N and 120°50′−121°45′E, belonging to the alluvial plain of Yangtze River Delta, to the west of the Yangtze River estuary, with a total area of approximately 8,239 km^2, covering eighteen districts and one county. Shanghai has experienced rapid urbanization at an unprecedented pace since its economic reform in the early 1990s. The urban built-up region covered an area of about 176 km^2 in 1984, and then expanded to an area covering 412 km^2 and 886 km^2 in 1996 and 2008, respectively.

Research on UHI effect accompanied by urban expansion in Shanghai has been driven by an increased concern for the area by the scientific community. Zhou et al. (2001) used NOAA/AVHRR data to analyze the distribution characteristics of thermal field and monitor its dynamic change in Shanghai. They also developed the correlation models of bright temperature and air temperature. Yan and Deng (2004) extracted LST, NDVI, and surface albedo from NOAA/AVHRR data, and analyzed heat island effect of Shanghai city during daytime and nighttime in summer and winter and the correlation between LST and other land surface parameters. Based on LST retrieved from Landsat TM6 and ETM+ 6 data of Shanghai central city from 1989 to 2002, Dai et al. (2010) quantitatively described the characteristics of spatial heterogeneity and temporal evolution of land surface thermal landscape at different scales and periods in Shanghai central city by utilizing Exploratory Spatial Data Analysis (ESDA). The results show that LST field in the city tends to fragmentize and becomes more problematic as Shanghai continues to develop, and while its global spatial difference gradually increases.

In recent years, the UHI in Shanghai has created new detrimental characteristics. For instance, the average maximum temperature of urban areas shows an evident rising trend, the heat island effect is intensifying in summer, extreme heat occurs frequently, and the centers of the heat island drift about with multiple centers emerging in the UHI (Qi, 2004; Yang et al., 2010). Consequently, more empirical research is required to investigate deeply into the characteristics of UHI in Shanghai, which has been experiencing a notable change of land use structure.

2.2 Data sources

2.2.1 Remotely sensed data

The remotely sensed dataset used here was acquired by the Moderate Resolution Imaging Spectroradiometer (MODIS) sensor, which was carried on National Aeronautics and Space Administration's (NASA's) Terra satellite launched on December 18, 1999, and later on the Aqua satellite launched on May 4, 2002. The MODIS instrument acquires data in 36 spectral bands between 0.4 μm and 14.4 μm with spatial resolutions of 250 m (2 bands), 500 m (5 bands), and 1,000 m (29 bands). In this research, the daily MODIS/Terra and Aqua Level 1B data products, including MOD021KM, MYD021KM, MOD02QKM, and MYD02QKM, were collected over the Shanghai area in January, April, July, and October 2007 and 2008. The MOD021KM (Terra) and MYD021KM (Aqua) data contain calibrated radiances from MODIS bands 8−36 (0.405−14.385 μm) at 1 km resolution and MODIS bands 1−7 (0.459−2.155 μm), each aggregated to appear at 1 km resolution. The MOD02QKM (Terra) and MYD02QKM (Aqua) data contain calibrated radiances from MODIS band 1 (0.620–0.670 μm) and band 2 (0.841–0.876 μm) at 250 m resolution. During these four

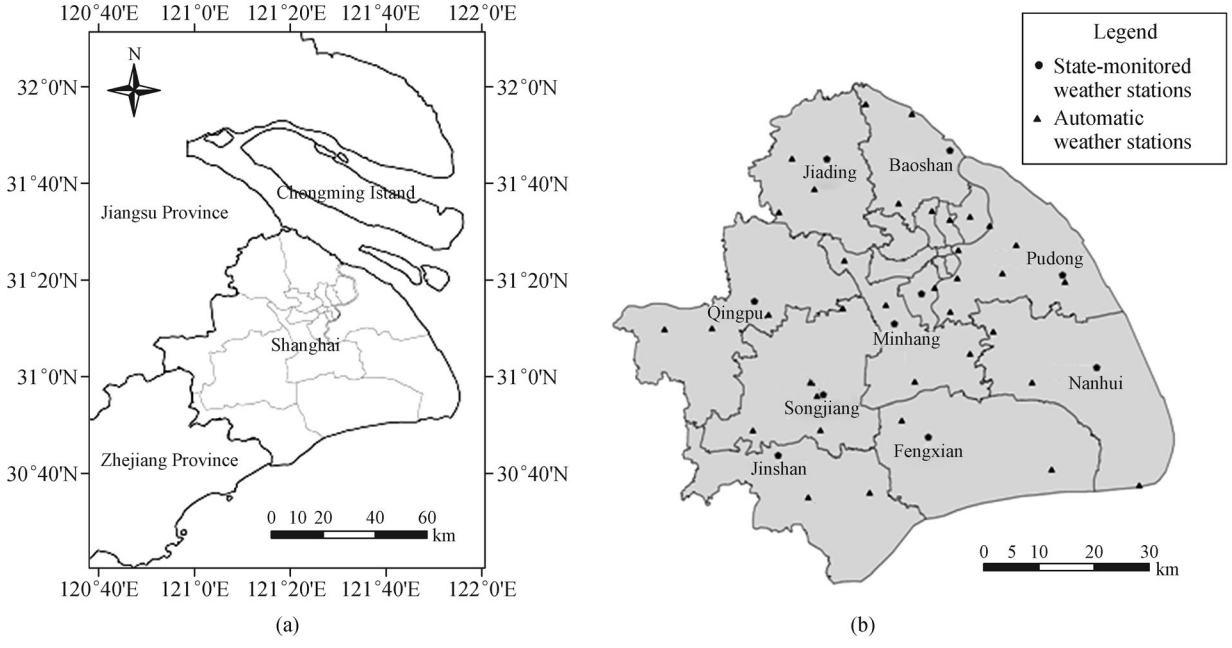

Fig. 1 Map of the study area (a) and location of state-monitored weather stations and automatic weather stations (b).

months in 2007 and 2008, 28 cloud-free MODIS images were selected. The amount of MODIS images used to retrieve LST are summarized in Table 1.

Table 1 Number of MODIS images used in this research

Year	January	April	July	October
2007	2	7	3	6
2008	2	3	3	2
Total	4	10	6	8

2.2.2 Meteorological data

In addition to satellite data, meteorological observations that were measured by 10 state-monitored weather stations during January, April, July, and October of 2007–2008 were collected. The dataset contained air temperature, wind speed, and LST measured at 02:00, 08:00, 14:00, and 20:00. In addition, measurements of air temperature and wind speed during the above study period were collected from 39 automatic weather stations. The meteorological data measurements were used to explore the relationship between air temperature and retrieved MODIS LST in winter, spring, summer, and autumn, respectively.

3 Retrieval of LST and its correlation with air temperature

3.1 LST retrieval from MODIS data

The existing methods for retrieval of LST from thermal infrared channel data of remotely sensed images can be classified into three categories: single-channel algorithm, split-window algorithm, and multi-band algorithm. In this paper, LST was retrieved from MODIS data by using the split-window algorithm proposed by Qin et al. (2005), which uses the data of two adjacent thermal infrared bands, i.e., band 31 and band 32, ranging in wavelength from 10.78 μm to 11.28 μm and 11.77 μm to 12.27 μm. The main process involved the estimation of spectral radiance from digital numbers (DNs) of bands 31 and 32, conversion of the radiance into brightness temperature, and computation of LST from brightness temperature. In this method, atmospheric water vapor content can be estimated using the equation developed by Mao and Qin (2004), and vegetation coverage can be estimated using the method proposed by Qin et al. (2004). In addition, the thermal radiation interaction between the vegetation and soil was estimated using the empirical equations proposed by Sobrino et al. (2004).

Terra satellite platform overpasses at approximately 10:30 and 22:30 local solar time, while Aqua satellite platform overpasses at approximately 13:30 and 01:30 local solar time. The LST retrieved from MODIS/Terra and Aqua data was compared with daily LST measured from 10 state-monitored weather stations at 08:00 and 14:00 in January, April, July, and October 2007 (Fig. 2). It can be seen from Fig. 2 that the retrieved MODIS LST data around 10:30 local time were all within the range of measured LST at 08:00 and at 14:00.

3.2 Correlation between air temperature and retrieved MODIS LST at 1 km resolution

3.2.1 Correlation analysis on annual scale

The air temperature measured at 08:00 and 14:00 at 49 weather stations, including 10 state-monitored weather stations and 39 automatic weather stations, was linearly interpolated to estimate the air temperature at the satellite passing time. The locations of 49 weather stations are shown in Fig. 1. On the other hand, the retrieved LST data were extracted at the locations of 49 weather stations. The relationship between these two types of data in January, April, July, and October 2007 and 2008 was studied through the bivariate correlation analysis. The significance of the three correlation coefficients (R^2) was determined by using a one-tail test (Table 2). The Pearson's correlation coefficient has significant advantages for continuous non-normal data which do not have obvious outliers (Chok, 2010). If the data contain outliers in one of both of the continuous variables, Spearman's rank-order correlation coefficient is considered more appropriate. Similar to Spearman's rank-order correlation coefficient, Kendall's tau correlation coefficient is designed to capture the association between two ordinal (not necessarily interval) variables. Similar to the two previous correlation coefficients, Kendall's tau ranges from -1 to $+1$, with its absolute value indicating the strength of monotonic relationship between the two variables (Chen and Popovich, 2002). However, Kendall's tau can be one for even a wider range of scenarios than Spearman's correlation coefficient. Due to the different nature of these three correlation coefficients in this research, a comprehensive analysis of the relationship between MODIS LST and air temperature was made using these correlation coefficients. Table 2 shows that the retrieved MODIS LST and interpolated air temperature have a high correlation with the Pearson's correlation coefficient of 0.836. These results demonstrate the potential for deriving air temperature data from retrieved LST.

3.2.2 Correlation analysis for four seasons

Due to the difference in solar radiation and vegetation coverage during each season, the correlations between LST and air temperature during different seasons were further studied in this research. January, April, July, and

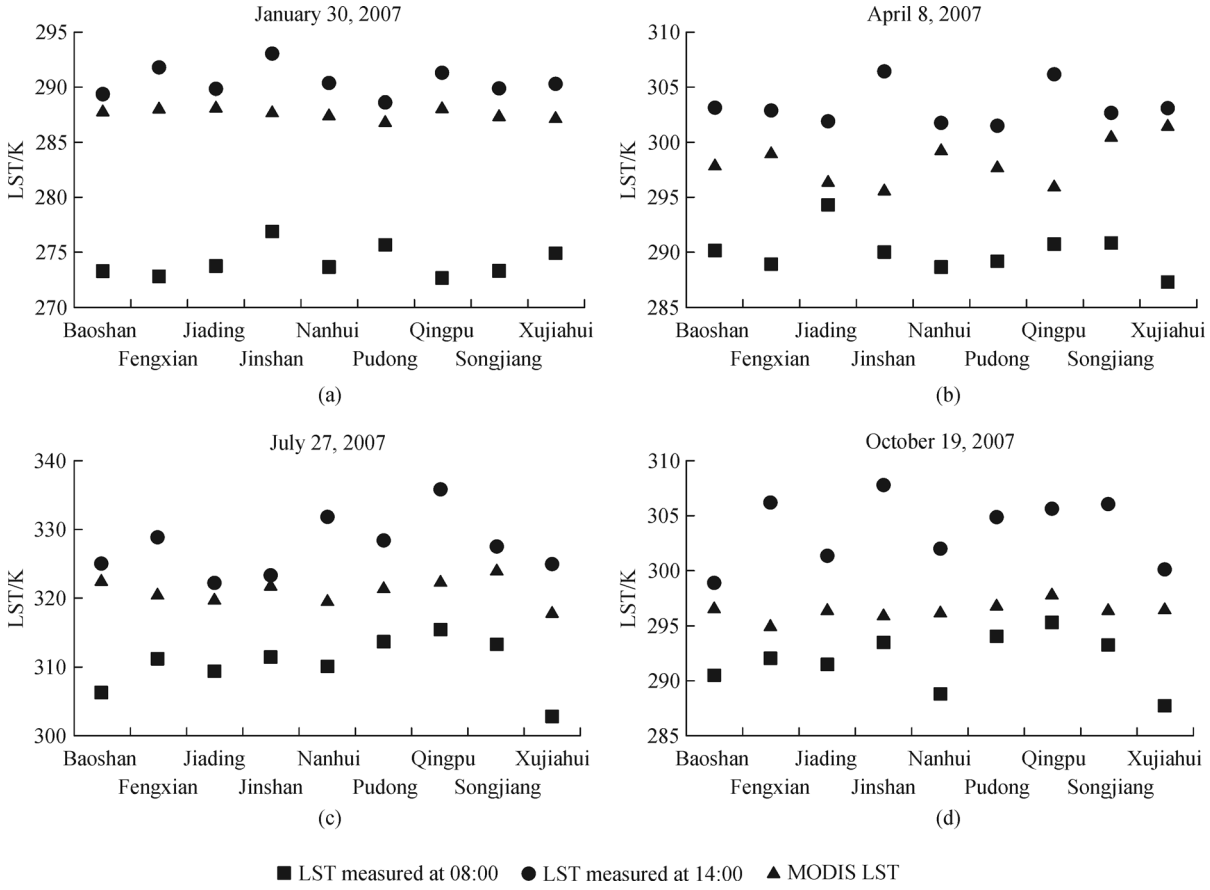

Fig. 2 Comparisons between LST measured from 10 state-monitored weather stations and retrieved MODIS LST at 11: 00 on January 30, 2007 (a), at 10:35 on April 8, 2007 (b), at 10:45 on July 27, 2007 (c), and at 10:20 on October 19, 2007 (d).

Table 2 Correlation coefficientsbetween air temperature and MODIS LST at 1 km and 250 m resolutionsin 2007 and 2008

Correlation coefficients	1 km resolution	250 m resolution
Pearson's correlation coefficient	0.836**	0.865**
Kendall's tau-b correlationcoefficient	0.571**	0.575**
Spearman's rho correlationcoefficient	0.768**	0.789**

** Correlation is significant atthe 0.01 level (one-tailed).

October were taken as representative months of winter, spring, summer, and autumn, respectively.

The results of bivariate correlation analysis revealed distinct differences in correlation coefficients (R^2) between LST and air temperature during different seasons (Table 3). The correlation coefficient was highest in autumn (October) with the Pearson's coefficient of 0.828, while the correlation coefficient was lowest in summer (July) with the Pearson's coefficient of 0.131. Consequently, air temperature displays a substantial correlation with the retrieved LST in autumn and spring in Shanghai; however, there are weaker correlations between LST and air temperature in summer and winter.

3.3 Correlation between air temperature and retrieved LST at 250 m resolution

3.3.1 Derivation of higher resolution LST data

Weather stations use sets of air temperature measurements at various observation points to collect their data, while the retrieved MODIS LST is in raster-based format with a spatial resolution of 1 km. There is a significant difference in spatial scale between these two types of data. To improve the accuracy of air temperature estimated from LST, the spatial resolution of retrieved LST was increased from 1 km to 250 m by applying the TsHARP algorithm

proposed by Agam et al. (2007) to MODIS thermal maps at 1 km resolution. Based on the assumption that a unique relationship between radiometric surface temperature and vegetation index exists at multiple resolutions, this algorithm can be used to sharpen thermal imagery to higher resolutions associated with the shorter wavebands (visible and near-infrared) used to compute vegetation indices. The parameters of the sharpening function in TsHARP are determined within the context of the scene to be sharpened, and thus reflect the local relationship between surface temperature and vegetation cover fraction. Further details on TsHARP algorithm can be found in Agam et al. (2007). By combining the retrieved 1 km MODIS LST images at 1 km resolution with shortwave Normalized Difference Vegetation Index (NDVI) data with 250 m resolution, the LST images at 250 m resolution were generated in this research.

3.3.2 Correlation at multiple time scales

The bivariate correlation analysis was conducted in 2007 and 2008 on the measured air temperature and retrieved LST data at a spatial resolution of 250 m. According to the Pearson, Kendall, and Spearman results of correlation coefficients (R^2) , the correlation between air temperature and retrieved LST is slightly higher at a 250 m resolution than at a 1 km resolution (see Table 2). Consequently, the same results came be assumed at annual scales.

The relationship between air temperature and retrieved MODIS LST in each season was also studied at 250 m resolution (Table 4). The results show that the Pearson's correlation coefficients are higher in spring (April) and autumn (October) at 250 m resolution than those at 1 km resolution, indicating that the fitting using the retrieved LST at 250 m resolution can derive the air temperature data with higher accuracy in spring and autumn. Alternatively, the coefficients of Kendall's tau-b and Spearman's rho show a lesser variance in these seasons, because these two coefficients are more suitable for detecting the correlation between the rank variables than the Pearson's correlation coefficient.

However, in summer (July) and winter (January), the correlation coefficients at 250 m resolution were lower than those at 1 km resolution. This result may be due to the fact that the accuracy of the TsHARP method decreases when the difference in NDVI of underlying surface increases (Agam et al., 2007). In summer, the high heterogeneity of NDVI distributed over the Shanghai terrestrial area may significantly influence the accuracy of retrieved LST using the TsHARP method, and consequently, may result in negative correlation coefficients in summer. In addition, the variable meteorological conditions that occur in Shanghai during summer and winter make it unfeasible to derive air temperature from retrieved MODIS LST at 250 m resolution.

4 Estimation of air temperature from retrieved MODIS LST

There is a high correlation between air temperature and the retrieved MODIS LST on an annual scale in Shanghai; however, this correlation ranges between weak and very weak in summer and winter, with an extremely strong correlation in spring and autumn. These dissimilarities are likely due to the variable meteorological fields, their complex influencing factors in summer and winter, and their relatively stable atmospheric structure in spring and autumn. Light wind typically prevails in Shanghai in spring and autumn, with relatively stable atmospheric

Table 3 Correlation coefficients between air temperature and MODIS LST at 1 km resolution during different seasons

Month	Pearson's correlation coefficient	Kendall's tau-b correlation coefficient	Spearman's rho correlation coefficient
January	0.362**	0.195**	0.338**
April	0.663**	0.475**	0.669**
July	0.131*	0.146**	0.226**
October	0.828**	0.416**	0.587**

** Correlation is significant at the 0.01 level (one-tailed). * Correlation is significant at the 0.05 level (one-tailed).

Table 4 Correlation coefficients between air temperature and MODIS LST at 250 m resolution during different seasons

Month	Pearson's correlation coefficient	Kendall's tau-b correlation coefficient	Spearman's rho correlation coefficient
January	0.299**	0.073	0.140*
April	0.683**	0.447**	0.649**
July	−0.464**	−0.266**	−0.391**
October	0.841**	0.474**	0.639**

** Correlation is significant at the 0.01 level (one-tailed). * Correlation is significant at the 0.05 level (one-tailed).

stratification; yet the weather changes frequently in summer, as influenced by a subtropical high, low-pressure trough and typhoon conditions. Furthermore, during the last decade, variances in air temperature during summer and winter have increased due to a higher frequency of extreme high-temperature in summer, and a gradual decrease in the number of low-temperature days in winter (Shi et al., 2009; Zhang et al., 2010).

Based on the correlation analyzed above, linear regression equations for estimating air temperature were constructed using air temperature measured from 49 weather stations and the retrieved MODIS LST at 250 m resolution in April and October of 2007 and 2008. As seen in the linear regression equations listed in Table 5, x denotes the retrieved LST (Unit: K), y denotes the air temperature measured from weather stations (Unit: K), and the resultant coefficients of determination (R^2) are 0.566 and 0.707 in April and October, respectively. As seen in related research studies, the determination coefficients (R^2) of linear regression for deriving air temperature using retrieved LST generally range from 0.55 to 0.70 (Jones et al., 2004; Liu et al., 2010; Fu et al., 2011), thus showing good accuracy in linear estimation of air temperatures from MODIS LST data in spring and autumn. The results of air temperature derived from retrieved MODIS LST data using the regression equations listed in Table 5 are illustrated in Fig. 3.

Table 5 The fitting equations to estimate air temperature

Seasons	Fitting equations	R^2
Spring (April)	$y = 0.309x + 198.634$	0.566^{**}
Autumn (October)	$y = 0.386x + 178.990$	0.707^{**}

** Correlation is significant at the 0.01 level (one-tailed).

5 Spatial distribution of air temperature thermal field

5.1 General characteristics of air temperature spatial distribution

According to the estimation results of air temperature as seen in Fig. 3, the highest and lowest air temperatures in Shanghai were 291.19 K and 287.92 K at 10:35 on April 8, 2007, with a heat island intensity of 3.27 K. On April 10, 2008, the highest and lowest air temperatures in Shanghai were 291.60 K and 287.32 K at 10:35, with a heat island intensity of 4.28 K. The estimated air temperature decreases gradually in circularity from the high temperature kernel observed in the downtown area to the urban fringe, which forms obvious UHI effect.

Figure 3 represents the general pattern of air temperature spatial distribution in Shanghai. In April, 2007, the thermal kernel zone was concentrated in the central urban area, and the high air temperature zones were mainly distributed over the districts of Baoshan and Pudong, adjacent to the thermal kernel zone. In April, 2008, the high air temperature zones extended northward and eastward, with a slightly increased area ratio of high air temperature zones observed in the districts of Jiading, Minhang, and Nanhui. The relatively lower air temperature zones were mainly distributed over the districts to the west of Shanghai, such as Jinshan, Songjiang, and Qingpu, in spring. The air temperature increased gradually from the southwestern to the northeastern areas, with the high temperature kernel located in the downtown area of Shanghai. Moreover, the UHI in Shanghai was characterized by a distribution pattern of multiple centers, with the central urban area as the primary center and the built-up regions in each district as the sub-centers in a thermal field in April 2007 and 2008.

The highest and lowest air temperatures in Shanghai were 293.24 K and 290.48 K at 10:20 on October 19, 2007, with a heat island intensity of 2.76 K. On October 15, 2008, the highest and lowest air temperatures in Shanghai were 294.70 K and 291.27 K at 11:00 with a heat island intensity of 3.43 K. Even though the heat island intensity in October is lower than in April, the UHI effect also apparently exists in autumn. The thermal kernel zone and high air temperature zones were mainly concentrated in the central urban area and its surroundings, encompassing a much smaller area than in April, 2007 and 2008. The relatively lower air temperature zones were mainly distributed over the districts west of Shanghai, such as Jinshan, Songjiang, and Qingpu, and to the south, such as Nanhui and Fengxian. There was a significant difference in air temperature between the northern and the southern regions, with higher air temperatures in the north and lower air temperatures in the south. Furthermore, the characteristic that the central urban area was the primary center in a thermal field was more evident in October than in April, while the multi-central distribution characteristic was less apparent in October.

According to the estimation of air temperature during the study period, the heat island intensity ranges from 3 K to 4 K in Shanghai, with a slightly higher intensity in spring than in autumn. The higher air temperature zone is generally concentrated in the central urban area northeast of Shanghai in spring and autumn, with a slightly larger in spring than in autumn. Alternatively, the lower air temperature zones are distributed in the southwestern region in spring and the southern region in autumn.

5.2 Comparison of air temperature thermal field during the study period

To make a quantitative comparison of UHI during different seasons and years, the normalized value (N) of air temperature was calculated for each pixel using the method proposed by Xu and Chen (2004). The greater the normalized value, the more intense the UHI. The

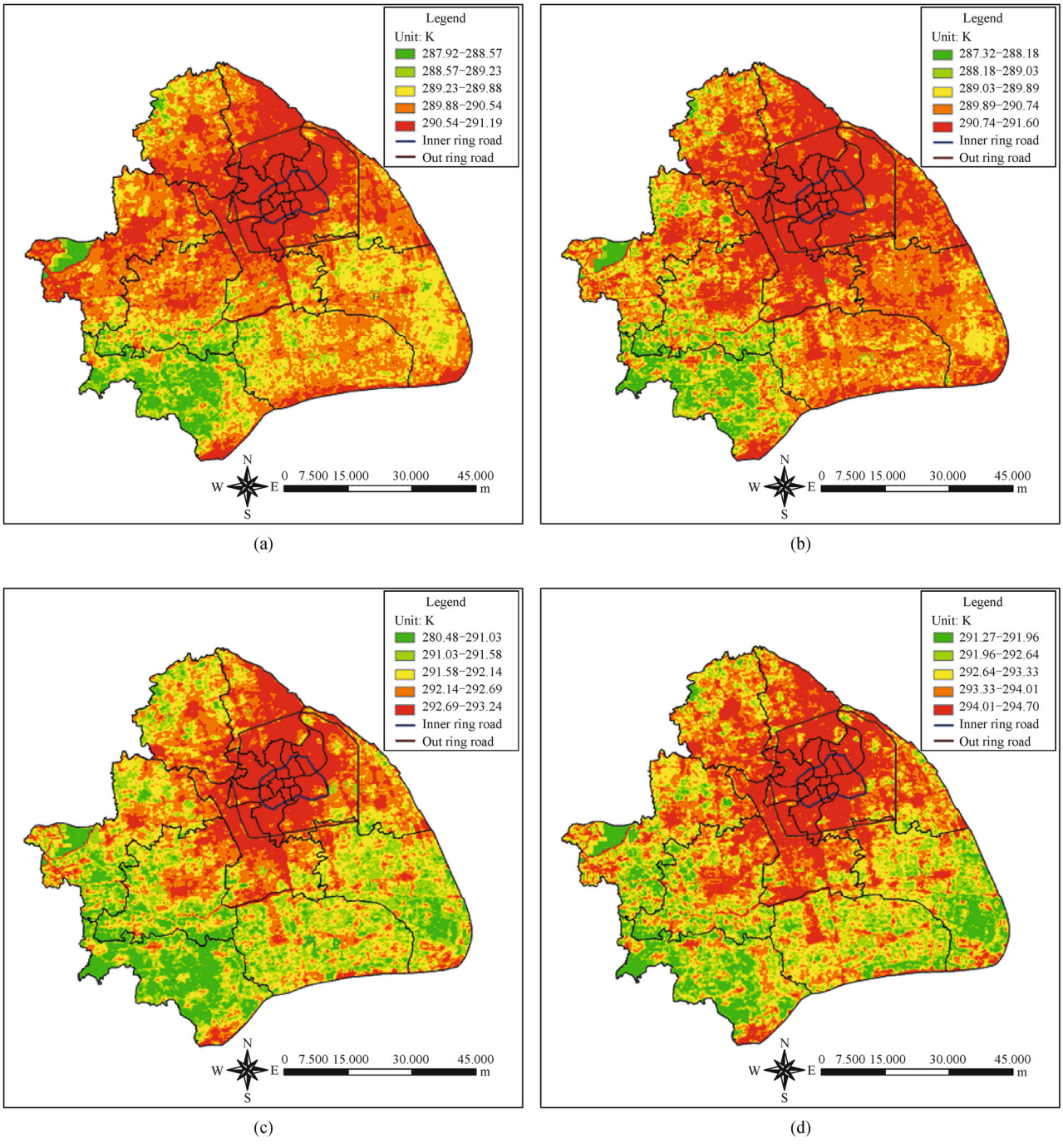

Fig. 3 Spatial distribution of air temperature derived from MODIS LST at 10:35 on April 8, 2007 (a), at 10:35 on April 10, 2008 (b), at 10:20 on October 19, 2007 (c), and at 11:00 on October 15, 2008 (d).

resultant multi-temporal normalized images (Fig. 4) were divided into five levels. The statistical results are presented in Table 6.

As shown in Table 6, the area of thermal kernel zone ($0.8 < N < 1.0$) and high air temperature zone ($0.6 < N < 0.8$) is larger in spring (April) than in autumn (October). The area at these two levels accounts for more than 60% of the total terrestrial area of Shanghai in April, and more than 40% in October, indicating a high coverage of UHI. The area of medium air temperature zone ($0.4 < N < 0.6$) and low air temperature zone ($0.2 < N < 0.4$) ranges from 23% to 45%. The area at these two levels is smaller in April than in October, reflecting that the coverage of higher air temperature is

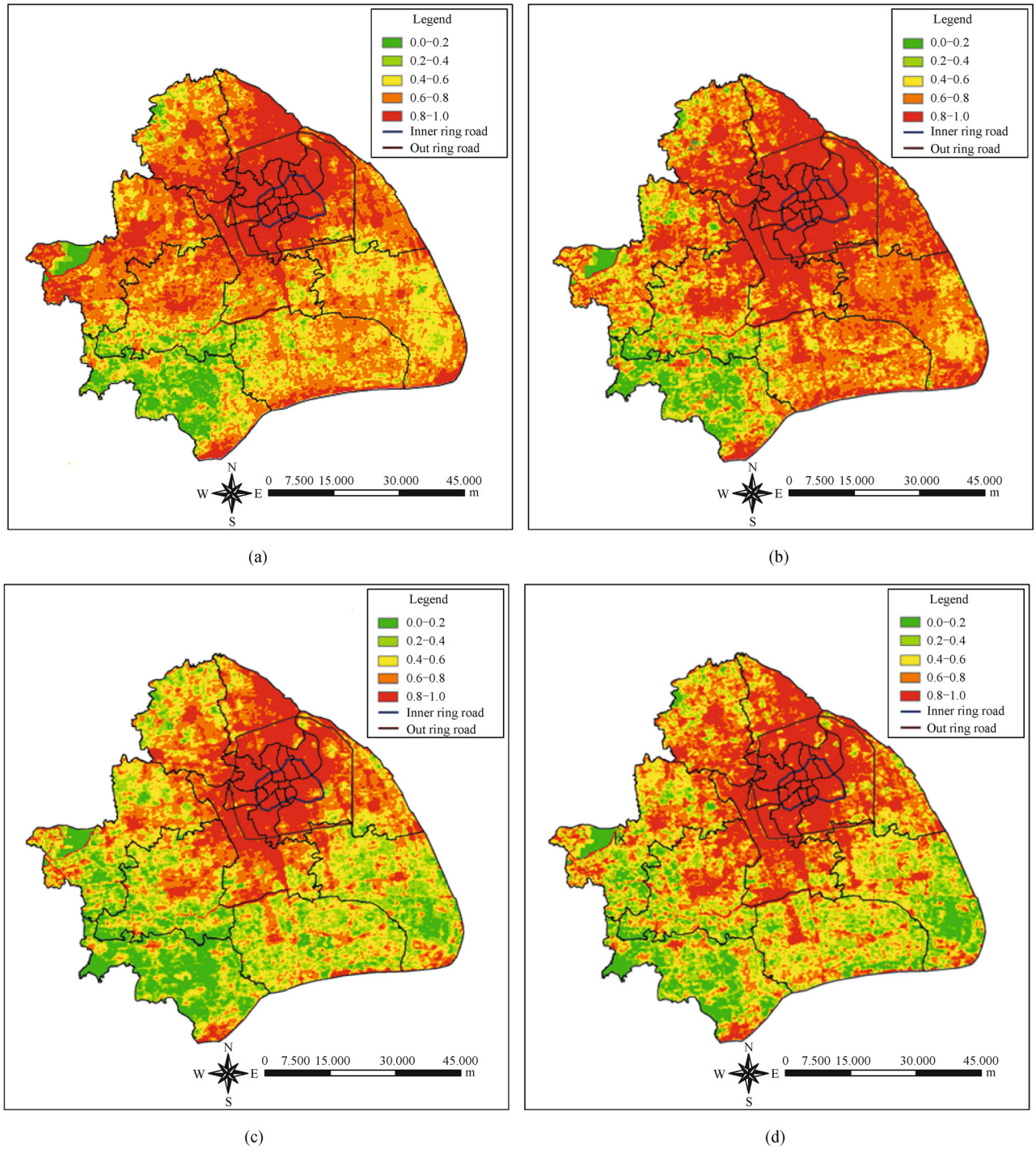

Fig. 4 Spatial distribution of normalized air temperature on April 8, 2007 (a), on April 10, 2008 (b), on October 19, 2007 (c), and on October 15, 2008 (d).

lower in autumn than in spring. The area of low air temperature zone ($N < 0.2$) is smallest with approximately 5.5% in April and 11% in October. These regions are mainly distributed over a large area of water and vegetation.

6 Comparison between LST and air temperature thermal field

In general, the maximum value of LST is always considerably higher than that of simultaneous air

Table 6 Proportion of different levels of normalized air temperature during the study period

Normalized value (*N*)	April 8, 2007/%	April 10, 2008/%	October 19, 2007/%	October 15, 2008/%
0.0−0.2	5.78	5.51	12.58	10.06
0.2−0.4	7.01	6.39	17.86	14.86
0.4−0.6	23.43	17.13	26.22	25.49
0.6−0.8	38.77	37.28	24.53	26.37
0.8−1.0	25.00	33.69	18.82	23.22

temperature in Shanghai, and the LST difference is also much larger than the difference in air temperature. According to the research on the thermal environment of land surface in Shanghai with multi-temporal remote sensing images (Chen et al., 2011), the area of low and lower air temperature zones is similar to that of low and lower LST zones, while the area of higher air temperature zones is larger than that of higher LST zones.

In air temperature thermal field, the area ratios of higher air temperature zones are quite different in each district. The higher air temperature zones are concentrated in the central urban area, from which the heat island intensity gradually decreases. The characteristic that the central urban area is the primary center in air temperature thermal field is evident. However, in LST thermal field, the difference in area ratios of higher LST zones is relatively smaller in different districts. The distribution of LST thermal field presents multi-central feature. The higher LST zones are scattered in the town centers, where are clustered with population, buildings, industrial zones, etc.

The above analyses indicate that there is significant difference in spatial distribution characteristics between air temperature thermal field and LST thermal field. The changes of underlying surface usually create a more immediate effect on LST thermal field, and afforestation, urban expansion and adjustment of industrial layout will influence the spatial pattern of LST thermal field directly. Consequently, the distribution of LST thermal field presents obvious multi-central feature, while the characteristic that the central urban area is the primary center is more evident in air temperature thermal field.

7 Conclusions

In this paper, the LST field of Shanghai city was retrieved from MODIS/Terra and Aqua data in 2007 and 2008, and the relationship between retrieved LST and interpolated air temperature measured from 49 weather stations was studied through the correlation analysis. The Pearson's correlation coefficient of 0.836 indicates that the retrieved MODIS LST and interpolated air temperature have a strong correlation on an annual scale. In spring and autumn, there is high correlation between air temperature and retrieved LST, while there is weak correlation in summer and winter. Furthermore, the spatial resolution of retrieved MODIS LST was increased from 1 km to 250 m by applying the TsHARP algorithm. Compared with the correlation coefficients computed using LST at 1 km resolution, there is a slightly higher correlation between air temperature and retrieved LST at 250 m resolution in spring and autumn, and on an annual scale. These results demonstrate the potential for estimating the distribution of air temperature thermal field from the retrieved MODIS LST at 250 m resolution in spring and autumn in Shanghai.

According to the estimation results of air temperature, the heat island intensity usually ranges from 3 K to 4 K in Shanghai, with a slightly higher intensity in spring than in autumn. The higher air temperature zones are mainly distributed over the central urban area, and the districts of Baoshan, Pudong, and Minhang, while the lower air temperature zones are mainly distributed over the districts of Fengxian, Nanhui, and Jinshan. The spatial distribution of the air temperature field is consonant with that of the built-up area ratio as a whole. Furthermore, the UHI in Shanghai is characterized by a distribution structure of a primary center (i.e., the central urban area), and multiple sub-centers (i.e., the built-up regions in each district).

The distribution pattern of the air temperature thermal field varies in different seasons. The area of higher air temperature zones, concentrated northeast of Shanghai, is larger in spring than in autumn. Alternatively, the lower air temperature zones are concentrated in the southwestern region in spring and southern region in autumn. There is a greater difference in the area ratio of higher air temperature zones between each district in autumn than in spring. The distribution characteristic of UHI designating the central urban area as the primary center in a thermal field is more evident in autumn.

The results obtained with MODIS land surface temperature data indicate that the method proposed in this paper can successfully produce spatial distribution maps of air temperature with 250 m resolution in spring and autumn in Shanghai. However, this method is unable to derive air temperature with 250 m resolution in summer and winter due to the low correlation between air temperature and MODIS LST. Therefore, the focus for future work will be the development of linear or nonlinear models to estimate the distribution of an air temperature thermal field from MODIS LST in summer and winter by

integrating with the parameters reflecting the spatial heterogeneity of urban land cover and variable meteorological conditions. In addition, because the vegetation index based TsHARP algorithm for spatial sharpening of thermal imagery is suitable for enhancement of the thermal information over agricultural regions, the thermal image sharpening technique will be improved to make it quite applicable to urban areas in further research.

Acknowledgements The work described in this paper was funded by the National Natural Science Foundation of China (Grant No. 41001234), National Statistical Science Foundation of China (No. 2012LZ001).

References

Agam N, Kustas W P, Anderson M C, Li F, Neale C M U (2007). A vegetation index based technique for spatial sharpening of thermal imagery. Remote Sens Environ, 107(4): 545–558

Chen M, Zhang H, Tang J, Chen W, Zhang Y, Ma W (2011). Study on the thermal environment of land surface in shanghai with multi-temporal remote sensing images. China Environ Sci, 31: 1143–1151

Chen P Y, Popovich P M (2002). Correlation: Parametric and Nonparametric Measures. Thousand Oaks, CA: Sage Publications

Chok N S (2010). Pearson's Versus Spearman's and Kendall's Correlation Coefficients for Continuous Data. Pittsburgh: University of Pittsburgh

Colombi A, De Michele C, Pepe M, Rampini A (2007). Estimation of daily mean air temperature from MODIS LST in Alpine areas. EARSeL eProceedings, 6: 38–46

Dai X, Guo Z, Zhang L, Li D (2010). Spatio-temporal exploratory analysis of urban surface temperature field in Shanghai, China. Stochastic Environ Res Risk Assess, 24(2): 247–257

Fu G, Shen Z, Zhang X, Shi P, Zhang Y, Wu J (2011). Estimating air temperature of an alpine meadow on the northern Tibetan Plateau using MODIS land surface temperature. Acta Ecol Sin, 31(1): 8–13

Jang J D, Viau A A, Anctil F (2004). Neural network estimation of air temperatures from AVHRR data. Int J Remote Sens, 25(21): 4541–4554

Jones P, Jedlovec G, Suggs R, Haines S (2004). Using MODIS LST to estimate minimum air temperatures at night. In: 13th Conference on Satellite Meteorology and Oceanography. American Metereological Society, Norfolk, Virginia, 1–6

Liu F, Lu Y, Jiang L, Xin H, Zhang T, Lu X (2010). Correlation analysis between MODIS brightness temperature and surface temperature provided by meteorological station. Seismology and Geology, 32: 127–137

Mao K B, Tang H J, Wang X F, Zhou Q B, Wang D L (2008). Near-surface air temperature estimation from ASTER data based on neural network algorithm. Int J Remote Sens, 29(20): 6021–6028

Mao K, Qin Z (2004). Retrieval of water content of atmosphere in Bohai region by MODIS image. Remote Sensing Information, 76: 47–50

Owen T W, Carlson T N, Gillies R R (1998). An assessment of satellite remotely-sensed land cover parameters in quantitatively describing the climatic effect of urbanization. Int J Remote Sens, 19: 1663–1681

Qi L (2004). Trend analysis of midsummer high temperature and urban heat island effect in Shanghai over past 10 Years. Meteorological Science and Technology, 32: 433–437

Qi S, Wang J, Zhang Q, Luo C, Zheng L (2005). Study on the estimation of air temperature from MODIS data. Journal of Remote Sensing, 9: 570–575

Qin Z, Gao M, Qin X, Li W, Xu B (2005). Methodology to retrieve land surface temperature from MODIS data for agricultural drought monitoring in China. Journal of Natural Disasters, 14: 64–71

Qin Z, Li W, Xu B, Chen Z, Liu J (2004). The estimation of land surface emissivity for LANDSAT TM6. Remote Sensing for Land and Resources, 3: 28–36

Shi J, Cui L, Tian Z (2009). Climatic characteristics of high and low temperature and its effecting factors in Shanghai. Resources and Environment in the Yangtze Basin, 12: 1143–1148

Sobrino J A, Jiménez-Muñoz J C, Paolini L (2004). Land surface temperature retrieval from LANDSAT TM5. Remote Sens Environ, 90(4): 434–440

Sobrino J A, Oltra-Carrió R, Sòria G, Bianchi R, Paganini M (2012). Impact of spatial resolution and satellite overpass time on evaluation of the surface urban heat island effects. Remote Sens Environ, 117: 50–56

Stisen S, Sandholt I, Nørgaard A, Fensholt R, Eklundh L (2007). Estimation of diurnal air temperature using MSG SEVIRI data in West Africa. Remote Sens Environ, 110(2): 262–274

Weng Q (2009). Thermal infrared remote sensing for urban climate and environmental studies: methods, applications, and trends. ISPRS J Photogramm Remote Sens, 64(4): 335–344

Xu H, Chen B (2004). Remote sensing of the urban heat island and its changes in Xiamen City of SE China. J Environ Sci (China), 16: 276–281

Yan H, Deng L (2004). Character analysis of heat island in Shanghai city using remote sensing parameters. Journal of Tropical Meteorology, 20: 579–585

Yang F, Lau S S Y, Qian F (2010). Summertime heat island intensities in three high-rise housing quarters in inner-city Shanghai China: building layout, density and greenery. Build Environ, 45(1): 115–134

Zakšek K, Schroedter-Homscheidt M (2009). Parameterization of air temperature in high temporal and spatial resolution from a combination of the SEVIRI and MODIS instruments. ISPRS J Photogramm Remote Sens, 64(4): 414–421

Zhang G, Zhen X, Tan J, Yin J (2010). The analysis of the relationship between the air quality in Shanghai and surface pressure patterns and meteorological factors. Journal of Tropical Meteorology, 1: 124–128

Zhou H, Zhou C, Ge W, Ding J (2001). The surveying on thermal distribution in urban based on GIS and remote sensing. Acta Geogr Sin, 56: 189–197